

## Journal Pre-proofs

Ultrathin Co-Co LDHs nanosheets assembled vertically on MXene: 3D nanoarrays for boosted visible-light-driven CO<sub>2</sub> reduction

Weiye Chen, Bin Han, Yili Xie, Shujie Liang, Hong Deng, Zhang Lin

PII: S1385-8947(19)32934-1  
DOI: <https://doi.org/10.1016/j.cej.2019.123519>  
Reference: CEJ 123519

To appear in: *Chemical Engineering Journal*

Received Date: 10 September 2019  
Revised Date: 25 October 2019  
Accepted Date: 16 November 2019

Please cite this article as: W. Chen, B. Han, Y. Xie, S. Liang, H. Deng, Z. Lin, Ultrathin Co-Co LDHs nanosheets assembled vertically on MXene: 3D nanoarrays for boosted visible-light-driven CO<sub>2</sub> reduction, *Chemical Engineering Journal* (2019), doi: <https://doi.org/10.1016/j.cej.2019.123519>

This is a PDF file of an article that has undergone enhancements after acceptance, such as the addition of a cover page and metadata, and formatting for readability, but it is not yet the definitive version of record. This version will undergo additional copyediting, typesetting and review before it is published in its final form, but we are providing this version to give early visibility of the article. Please note that, during the production process, errors may be discovered which could affect the content, and all legal disclaimers that apply to the journal pertain.

© 2019 Published by Elsevier B.V.



# Ultrathin Co-Co LDHs nanosheets assembled vertically on MXene: 3D nanoarrays for boosted visible-light-driven CO<sub>2</sub> reduction

Weiye Chen<sup>a, b, #</sup>, Bin Han<sup>a, b, #</sup>, Yili Xie<sup>a, b</sup>, Shujie Liang<sup>a, b</sup>, Hong Deng<sup>a, b\*</sup>, Zhang Lin<sup>a, b</sup>

<sup>a</sup> School of Environment and Energy, Key Laboratory of Pollution Control and Ecosystem Restoration in Industry Clusters (Ministry of Education), South China University of Technology, Guangzhou 510006, China

<sup>b</sup> Guangdong Engineering and Technology Research Center for Environmental Nanomaterials, South China University of Technology, Guangzhou 510006, China

<sup>#</sup> These authors contributed equally to this work.

□ Corresponding author.

E-mail address: dengh2016@scut.edu.cn

**Abstract:** Converting carbon dioxide (CO<sub>2</sub>) to multiple energy-rich chemicals by photocatalysis could validly mitigate the severe issues of climate changes and energy shortages. Exploring efficient catalysts for enhancing the performance of CO<sub>2</sub> photoreduction is still challenging. Herein, a novel three-dimensional hierarchical Co-Co layered double hydroxide/Ti<sub>3</sub>C<sub>2</sub>T<sub>x</sub> nanosheets (Co-Co LDH/TNS) nanoarray was successfully prepared *via* an *in-situ* MOF-derived strategy. This wise design rationally integrates the functional and structural merits of active Co species with conductive MXene to a hierarchical nanoarray architecture composed of ultrathin nanosheets, which can remarkably promote separation of photogenerated charge carriers and accelerate electrons transmission. Benefitting from these features, the hierarchical Co-

Co LDH/TNS composites manifest significant enhancement on the CO<sub>2</sub>-to-CO evolving rate ( $1.25 \times 10^4 \mu\text{mol h}^{-1} \text{g}^{-1}$ ) under illumination (>400nm) with a high apparent quantum efficiency (0.92%) and excellent stability. Our work demonstrates that 3D hybrid structure composed of MXene species can serve as promising candidates for CO<sub>2</sub> photoreduction, providing fundamental guidance to improve photocatalytic performance by rational engineering of complex hierarchical architecture materials.

**Keywords:** CO<sub>2</sub> reduction; photocatalysis; hierarchical structure; Ti<sub>3</sub>C<sub>2</sub>T<sub>x</sub> nanosheets; electrons transfer;

## 1. Introduction

Recently, numerous studies have been focused on the photocatalytic reduction of CO<sub>2</sub> into value-added chemicals by inexhaustible solar energy, as is one of the most prospective ways for mitigating global warming and energy crisis simultaneously [1-7]. Generally, the main process of photoreduction CO<sub>2</sub> is that electron-hole pairs are excited by appropriate photons, from which the extracted electrons transport to the surface active sites to reduce the adsorbed CO<sub>2</sub> molecules [8, 9]. Obviously, the transmission of electrons to the active sites is one of the critical steps during the photocatalytic CO<sub>2</sub> reduction process. Transition metal ions (e.g., cobalt, nickel) with multiple redox states are advantageous ingredients to establish electron transmission chains for CO<sub>2</sub> reduction, which could validly avoid the generation of undesired high-energy intermediates and improve the multi-electrons CO<sub>2</sub> reduction, especially when the reaction is combined with protons [9-21]. Despite this, the efficiency of photo reduction CO<sub>2</sub> is still far from enough to achieve practical applications due to the rapid

recombination of electron-hole pair during photocatalysis and the insufficient active sites [22-27]. which significantly diminish the utilization of photoinduced electrons. Thus, to achieve better photoreduction CO<sub>2</sub> performance, developing suitable methods to promote the utilization of photoinduced electrons is urgently needed.

Introducing highly conductive substances into the photocatalytic system is one of the most powerful ways to solve the dilemma mentioned above [28]. MXenes have drawn enormous attention as a newly group of two-dimensional transition metal nitrides/carbides, since it was first found by Gogotsi et al. in 2011 [29]. Generally, MXenes are prepared by selective etching from the bulk MAX phase, where M indicates an early transition metal, A stands for group IIIA/IVA elements, and X is C/N elements [30, 31]. For instance, Ti<sub>3</sub>C<sub>2</sub>T<sub>x</sub> (T<sub>x</sub> represents the surface terminations), as one of the most investigated MXenes, is usually obtained by removing aluminum atom layers from Ti<sub>3</sub>AlC<sub>2</sub> with hydrofluoric acid (HF). Benefitting from the merits of large specific surface area, high conductivity, compositional variability, and good chemical stability [32, 33]. MXenes have been widely researched and applied in numerous fields, such as catalysis, supercapacitors, antibacterial films, and batteries [34-38]. The photocatalytic researches of MXene has also been reported. For example, previous studies found that photocatalytic H<sub>2</sub>-generation activity of CdS could be elevated through combination with Ti<sub>3</sub>C<sub>2</sub> owing to its excellent conductivity [39, 40]. On the basis of these, it is expected that the combination of transition metal compound and MXene could improve the photocatalytic CO<sub>2</sub> reduction performance, yet still in its infancy.

On the other hands, the achievement of superior photocatalytic properties also relies on the delicate designation and fabrication of properly structured catalysts, which benefits to taking full advantage of separated electrons [41, 42]. Among the various attainable nanostructures, 2D nanosheets have aroused growing attention in energy and environmental relevant catalytic fields owing to their large specific surface area and abundant exposed active sites [43-45]. Particularly, with regard to the photocatalytic process, the atomic-level thickness can validly shorten the distance for which electrons diffuse to the catalysts surface, thus enhancing the separation rate of charge carriers [10, 46]. These virtues of 2D materials are valuable for enhancing photoreduction  $\text{CO}_2$  performance compared to their corresponding bulk counterparts [47-50]. Particularly, constructing hierarchical nanoarray structures based on vertical sheets-on-sheets has demonstrated to be one of the most effective ways to elevate catalytic performance by the synergistic effects of exposing more catalytically active sites and accelerates the electrons transport to the active sites [51, 52]. Inspiring by the above benefits, materials with hierarchical nanoarray architecture composed of 2D structures and conductive substrates may manifest excellent properties in photocatalytic reaction.

Herein, we delicately synthesized Co-Co LDH/MXene nanoarrays through an in-situ MOF derived strategy, which converts ZIF-67 MOFs into 2D Co-Co LDH vertical on exfoliated  $\text{Ti}_3\text{C}_2\text{T}_x$  nanosheets, yielding Co-Co LDH/ $\text{Ti}_3\text{C}_2\text{T}_x$  nanosheets hybrids (Co-Co LDH/TNS). Subsequently, the obtained Co-Co LDH/TNS composites were employed as cocatalysts for photocatalytic  $\text{CO}_2$  reduction with Ru-based photosensitizers. This successfully fabricated hybrids feature a highway for electron

transfer due to the synergistic effects of distinctive hierarchical structures and superior conductive MXene species. Thus, as compared with pristine Co-Co LDH, the composites display significant enhancement on photocatalytic CO<sub>2</sub> reduction performance, accompanied by the excellent stability and a high value of apparent quantum efficiency. This work provides a novel avenue for constructing MXenes-based 3D nanoarrays for boosted photocatalytic CO<sub>2</sub> reduction and could be extended to other environmental and energetic applications.

## 2. Experimental section

### 2.1 Chemicals

All the chemicals in our experiments were used as bought without further purification, containing cobalt nitrate hexahydrate (Co(NO<sub>3</sub>)<sub>2</sub>·6H<sub>2</sub>O, Aladdin, 99%), 2-Methylimidazole (2-MIM, Aladdin, 98%), anhydrous methanol (≥99.5%), [Ru(bpy)<sub>3</sub>]Cl<sub>2</sub>·6H<sub>2</sub>O (bpy: 2,2-bipyridine, Innochem, 98%), acetonitrile (MeCN, Aladdin, >99.5%), triethanolamine (TEOA, Aladdin, >99.0%), hydrofluoric acid (HF, Aladdin, 40% aqueous solution), tetrapropyl ammonium hydroxide (TPAOH, Macklin, 25wt.% aqueous solution), potassium hydroxide (KOH, Aladdin, 99%), ultra-purity CO<sub>2</sub> (99.999%) and ultra-purity Ar (99.9999%), the gas was purchased from Foshan Ms Messer Gas Co., Ltd. Ti<sub>3</sub>AlC<sub>2</sub> was purchased from Forsman Co., Ltd.

### 2.2 Synthesis of materials

Synthesis of Ti<sub>3</sub>C<sub>2</sub>T<sub>x</sub> nanosheets: The synthesis experiments were slightly modified based on the methods described in the previous literature [36]. First, 1 g Ti<sub>3</sub>AlC<sub>2</sub> powders were slowly immersed in 20 mL HF solution (≥ 40.0%) and then

stirred at 25 °C for 3 d. The suspension was separated by centrifugation and rinsed with distilled water until the  $\text{pH} \geq 6$ . Then, the obtained precipitation was re-dispersed in 50 mL TPAOH with magnetically stirring for 3 d at 25 °C. The mixture was gathered by centrifugation and rinsed with  $\text{H}_2\text{O}$  to remove the residual TPAOH. Afterward, the obtained sample was dispersed in  $\text{H}_2\text{O}$  and treated by ultrasonication under nitrogen atmosphere for 12 h. Finally, the suspension was centrifuged and freeze-dried to obtain the  $\text{Ti}_3\text{C}_2\text{T}_x$  nanosheets.

Synthesis of Co-Co LDH/TNS: Different quality (8 mg, 15 mg, 22 mg, 30 mg) TNS powder was sonicated in 15 mL methanol for 1 h. Subsequently, 0.546 g  $\text{Co}(\text{NO}_3)_2 \cdot 6\text{H}_2\text{O}$  was added into the above solution and stirred 2 h. Then, 0.616 g 2-MIM was dissolved in 15 mL methanol and mixed with the  $\text{Co}(\text{NO}_3)_2/\text{TNS}$  solution. The mixture was treated by ultrasonication for 0.5 h and stirred for 2 h. After ten minutes of centrifugation, the resultant solids were re-dispersed in 15 mL methanol and mixed with  $\text{Co}(\text{NO}_3)_2$  solution (15 mL methanol including 0.546 g  $\text{Co}(\text{NO}_3)_2$ ). Afterward, the mixture solution was poured into Teflon-lined stainless-steel autoclaves and held at 120 °C for 1 h. Finally, the dark green products were collected by centrifugation, washed with methanol several times, and vacuum dried at 65 °C for further use. To make the text more readable, the names of the Co-Co LDH/ $\text{Ti}_3\text{C}_2\text{T}_x$  nanosheet mixtures can be abbreviated as Co-Co LDH/TNS-8, Co-Co LDH/TNS-15, Co-Co LDH/TNS-22, Co-Co LDH/TNS-30, respectively, where the suffix indicates the amount of TNS powder added during the synthesis. In order to obtain pure Co-Co LDH for comparison, the procedure was similar to the synthesis process of Co-Co LDH/TNS

composite, without the addition of the TNS powder. In addition, pure Co-Co LDH and 15mg TNS were physically stirred at room temperature for 24 hours in 50ml distilled water, then the sample was gathered by centrifugation and vacuum dried, and the resulting two-dimensional composite was named " Co-Co LDH+TNS-15".

### 2.3 Materials characterization

X-ray diffraction (XRD) patterns were performed to investigate the crystal structure by Bruker D8 AVANCE X-ray diffractometer equipped with Cu K $\alpha$ . X-ray photoelectron spectroscopy (XPS) measurements were conducted by Thermo Fisher Scientific Escalab 250Xi X-ray photoelectron spectrometer employing Al K $\alpha$  radiation to characterize the surface ingredients of the resultant products. The morphologies and element distribution of the samples were recorded through field emission scanning electron microscopy (FE-SEM; Carl Zeiss MERLIN), transmission electron microscopy (TEM, JEM-2100, JEOL Ltd.) with elemental mapping, and high-resolution TEM (HRTEM). Raman spectra were operated on a Laser Raman spectrometer (LabRamHR, HORIBA Jobin Yvon. Co., France) at room temperature. An RX1 PerkinElmer Fourier transform infrared spectroscopy (FT-IR) spectrometer was used to investigate FT-IR spectrum. The nitrogen adsorption/desorption isotherms and porous structure information were measured on a Micromeritics ASAP 2020 analyzer accompanied with degassing for 8 h at 413 K before performing the sorption measurements. Then, we used a Brunauer-Emmett-Teller (BET) formula to calculate the specific surface area value. The weight percentage of metal elements were investigated by inductively coupled plasma optical emission spectrometer (ICP-OES,

Agilent 730). The UV-Vis absorption spectra/diffuse reflectance spectra (DRS) were carried out by a Shimadzu UV-2700 UV-Vis spectrophotometer with BaSO<sub>4</sub> as the reflectance standard. A Hitachi F-4600 tool was used to collect the photoluminescence (PL) spectra at room temperature under laser irradiation (540 nm). The above measurements were performed in a MeCN/H<sub>2</sub>O/TEOA solution (3 mL/2 mL/1 mL) including [Ru(bpy)<sub>3</sub>]Cl<sub>2</sub>·6H<sub>2</sub>O (7.5 mg). Electrochemical measurements were operated on an electrochemical workstation (CHI 660E). The prepared Ag/AgCl electrode (reference electrode), material-modified ITO glass (working electrode) and the Pt net (counter electrode) together form a typical three-electrode system in KOH solution (1M). Electrochemical impedance spectroscopy (EIS) data were investigated at the open-circuit voltage of 0 V in the frequency range of 1 Hz to 100 KHz, similarly, the tests were conducted in the acetonitrile/water/triethanolamine (3 mL/2 mL/1 mL) mixture solution. Mott–Schottky measurements were carried out at a constant frequency of 5 KHz, 10 KHz and 15 KHz between -0.8 V and 0.8 V. A zeta potential analyzer (NanoBrook Omni, American) was employed to measure the zeta potentials of TNS. The dosage of the sample was 1 mg·ml<sup>-1</sup>.

#### **2.4 Photocatalytic CO<sub>2</sub> reduction**

The photocatalysis performance was tested by combining the catalysts (0.5 mg) and the [Ru(bpy)<sub>3</sub>]Cl<sub>2</sub>·6H<sub>2</sub>O (7.5 mg) in a gas-closed quartz reactor which contains MeCN/H<sub>2</sub>O/TEOA (3 mL/2 mL/1 mL) mixture solution. Before illumination, the whole reaction device was vacuum degassed for 5 min, then we introduce the CO<sub>2</sub> gas (99.999%) into the reactor for about 15 min to replacement the air. Afterwards, we used

a 5W LED lamp (Beijing Perfect Light Company, China, 400 nm-1000 nm) as the light source. After a period of irradiation, a gas chromatography was used to detect the products (Agilent 7890B, CO was analyzed by flame ionization detectors and H<sub>2</sub> was analyzed by thermal conductivity detectors).

### 2.5 Apparent quantum efficiency values measurement

The apparent quantum efficiency (A.Q.E.) value was obtained under the monochromic light of 420 nm with a bandpass filter. The testing procedure was same as the photocatalytic reaction described above. An optical power meter (Ceaulight) was used to test the light intensity (32.3 mW·cm<sup>-2</sup> at 420 nm). And the illuminated area was about 3.0 cm<sup>2</sup>. Based on the Beer-Lambert's law, incident light was supposed to be completely absorbed. The value of A.Q.E. was determined by the following formula:

$$\text{A.Q.E.} = \frac{2nNh\nu c}{P\lambda t} * 100\%$$

Where n is the CO quantity. N is Avogadro constant. h is Planck constant. c is light velocity. P is light intensity.  $\lambda$  is light wavelength. t is the photoreduction reaction time.

## 3. Results and discussion

The synthetic process of the Co-Co LDH/TNS is schematically illustrated in Fig. 1. At first, the Al layers of the original Ti<sub>3</sub>AlC<sub>2</sub> bulk were etched by HF to obtain the accordion-shape Ti<sub>3</sub>C<sub>2</sub>T<sub>x</sub>, as showed in the Fig. S1a, b. After that, a TPAOH-intercalation assisted ultrasonic exfoliation method was conducted to yield the few-layer Ti<sub>3</sub>C<sub>2</sub>T<sub>x</sub> nanosheets (Fig. S1c). Also, the elementary mapping images clearly present that Ti, C, F, and O are uniformly distributed (Fig. S1d). Subsequently, the

resulting TNS played the role of a synthetic substrate to integrate with MOF derivatives. During the synthesis procedure, when we added TNS into  $\text{Co}(\text{NO}_3)_2$  solution,  $\text{Co}^{2+}$  were likely adsorbed on the TNS surface, which is ascribed to the negative potential of TNS ( $-24.2$  mV,  $\text{pH} = 7$ , Fig. S2) with numerous terminal functional groups (e.g.  $-\text{F}$  or  $-\text{OH}$ ). Afterward, the surface-anchored  $\text{Co}^{2+}$  could combine with 2-MIM to form ZIF-67 [53]. Finally, Co-Co LDH/TNS composites were obtained through a solvothermal process in the presence of  $\text{Co}^{2+}$ . For the probable fabrication mechanism,  $\text{H}^+$  derived from the hydrolysis of  $\text{Co}(\text{NO}_3)_2 \cdot 6\text{H}_2\text{O}$  could slowly etch ZIF-67 polyhedrons. The released  $\text{Co}^{2+}$  ions from the ZIF-67 would be partially oxidized by  $\text{NO}_3^-$  ions and dissolved  $\text{O}_2$ , then co-precipitates with  $\text{Co}^{2+}$  and  $\text{Co}^{3+}$  cations to form LDH structure [54]. Due to this delicate synthetic method, LDH nanosheets inherited the 3D architecture of ZIF-67, thus staggered standing on the TNS substrate to form a 3D nanoarray architecture (Fig. 2a), which is conducive to its high performance in  $\text{CO}_2$  photoreduction. A typical TEM image (Fig. 2b, Fig. S3a, b) of the as-formed material also presents strongly link for the composite, which is agreement with the SEM picture. The clear boundary between Co-Co LDH and TNS could be observed in the HRTEM image (Fig. 2c). Besides, the elementary mapping images explicitly elucidate that Co, Ti, and C elements are homogeneously distributed (Fig. 2d). All the above results strongly indicate the intimate and uniform binding between TNS and Co-Co LDH, namely, the successful fabrication of Co-Co LDH/TNS composites. Such composites are characterized with large contact area between each other, thus promoting the interfacial electron transfer during the photoreduction  $\text{CO}_2$  process. As a comparison,

pure Co-Co LDH sample holds a hollow structure which is directly evolved from ZIF-67 (Fig. S4a, b). The Co-Co LDH+TNS-15 hybrid obtained by physical stirring has a 2D/2D stack morphology (Fig. S5).

More detailed crystal structure and chemical composition analyses for the samples were performed. Fig. S6a displays the XRD patterns of the MXene. Obviously, after etching by the HF, the characteristic peaks of accordion-shape  $\text{Ti}_3\text{C}_2\text{T}_x$  at  $39^\circ$  is absent compared that of bulk  $\text{Ti}_3\text{AlC}_2$ , indicating the successful elimination of the Al layers [55,56]. Moreover, it could be found that the (002) diffraction peak of TNS moves to a lower angle after intercalated and exfoliated in comparison with accordion-shape  $\text{Ti}_3\text{C}_2\text{T}_x$ , which caused by the enlarged interlayer distance of the TNS [57]. The chemical composition of the bulk  $\text{Ti}_3\text{AlC}_2$  and the TNS were measured by XPS (Fig. S6b). Almost no peak of Al 2P could be observed in TNS, which is consistent with the conclusion pointed out by XRD analyses [36]. In Raman spectra (Fig. S6c), some appeared characteristic bands of  $\text{Ti}_3\text{AlC}_2$  are attributed to the Raman-active phonon vibration modes of  $\omega_1$ ,  $\omega_2$ ,  $\omega_3$  and  $\omega_4$ . However, it is worth noting that peak  $\omega_1$  and  $\omega_2$  of TNS are vanished, while peak  $\omega_3$  and  $\omega_4$  are broadened. Moreover, the  $\omega_3$  Raman band mode of TNS is downshifted in comparison with  $\text{Ti}_3\text{AlC}_2$ . Such shift proves the successful exfoliation of bulk phase to quite thin nanosheets, which is consistent with the previous research [53, 55]. As for Co-Co LDH/TNS hybrids, the diffraction peaks at  $11.5^\circ$ ,  $23.2^\circ$ ,  $34.5^\circ$ , and  $60.0^\circ$  in XRD patterns (Fig.3a) are correspond to the (003), (006), (012) and (015) planes of hydroxalite-like materials, respectively ( $\text{Co}_6\text{Al}_2\text{CO}_3(\text{OH})_{16}\cdot 4\text{H}_2\text{O}$ , JCPDS No.51-0045) [54]. suggesting the successful

transformation from ZIF-67 to Co-Co LDH. A series of controlled experiments were conducted with various TNS mass. The diffraction peak of TNS could not be obviously observed due to its low content relative to the Co-Co LDH, but for the Co-Co LDH/TNS-30 sample, a characteristic peak belonging to TNS (at *ca.* 5°) can be observed clearly. Otherwise, as the TNS quality increases, the peak intensity of the hybrid becomes weaker. The main reason is that the small particles at the bottom of LDH would uniformly coat on the TNS surface, which would result in the lower crystalline peaks intensity with increased amounts of TNS [54]. On the other hand, since the TNS has an extremely low diffraction peak intensity in the range of 10-70°, the peak intensity of the hybrids decreases as the relative contents of TNS increases. The above results signify the successful construction of Co-Co LDH/TNS hybrids. As presented in Table. S1, the weight percentage of Ti in the hybrid catalysts elevated with increased amounts of TNS, while Co exhibit opposite trends. XPS characterization was also conducted to prove the elements composition and valence states information in as-prepared hybrids and individual Co-Co LDH. As shown in Fig. 3b, all components (Co, O, Ti, and C) related to the Co-Co LDH/TNS-15 composite could be found in the survey spectrum. Furthermore, in the high-resolution spectra of Co 2p for Co-Co LDH (Fig. 3c), apart from the noticeable satellite peaks (named as “sat.”), the binding energies position at approximately 797.4, 782.2, 796.2 and 780.9 eV from the Co<sup>2+</sup> 2p<sub>1/2</sub>, Co<sup>2+</sup> 2p<sub>3/2</sub>, Co<sup>3+</sup> 2p<sub>1/2</sub> and Co<sup>3+</sup> 2p<sub>3/2</sub> spectrum, respectively, indicating the successful construction of Co-Co LDH [10]. Apparently, the core level orbitals locations of Co 2p peaks for Co-Co LDH/TNS-15 hybrids display 0.3 eV shifts, which exhibits a higher

binding energy than Co-Co LDH. The similar positive shift can be observed in Fig. 3d for the C 1s spectra. Otherwise, as for Raman spectra (Fig. S7), the peaks of the composites are also shifted relative to that of the pure Co-Co LDH. These results disclose strong interface interaction between Co-Co LDH and TNS [8]. Moreover, the FT-IR measurement (Fig. S8) demonstrated that nitrate anions are the main intercalated anions in Co-Co LDH.

The photoreduction CO<sub>2</sub> performances of all as-synthesized samples were investigated through visible light driven photocatalytic experiments conducted in an H<sub>2</sub>O/MeCN mixture solution under moderate conditions with [Ru(bpy)<sub>3</sub>]Cl<sub>2</sub>·6H<sub>2</sub>O and TEOA as the photosensitizer and sacrificial agent, respectively. CO and H<sub>2</sub> were the major products, consistent with the results in previous similar systems [10]. Fig. 4a presents the effects of TNS quality on photocatalytic activity. With increasing TNS content in the hybrids, photocatalytic CO<sub>2</sub> reduction activity enhance significantly in compared that of the pristine Co-Co LDH. Especially, the CO generation rate of the optimized sample Co-Co LDH/TNS-15 is 6.248 μmol h<sup>-1</sup> (1.25×10<sup>4</sup> μmol h<sup>-1</sup> g<sup>-1</sup>), which is 2.2 times that over Co-Co LDH. Such performance enhancement could be attributed to the rapid and efficient transmission of electrons through the interface of the hybrids [40, 58], which allows more adsorbed CO<sub>2</sub> at the cobalt active sites to be reduced. Noticeably, the individual TNS almost has no catalytic activity, so, excessive TNS in the hybrids will hinder the cobalt active sites with multiple redox states and lead to the decreased photocatalytic activity.

Series of comparative reactions were conducted to further explore the fundamental

impact factors determining the activity of the photoreduction catalysts. When the photoreduction  $\text{CO}_2$  experiment was employed with Co-Co LDH/TNS-15, the production rate and selectivity of CO are  $6.248 \mu\text{mol}\cdot\text{h}^{-1}$  ( $1.25\times 10^4 \mu\text{mol h}^{-1} \text{g}^{-1}$ ) and 63.9%, respectively, which are markedly higher than that of the no catalyst system ( $0.24 \mu\text{mol}\cdot\text{h}^{-1}$ , 37.7%) (Fig. 4b, columns 1 and 7). This phenomenon demonstrates that the catalyst plays a key role in the photocatalytic  $\text{CO}_2$  reduction system. Then, in the dark condition or the absence of photosensitizer, no gas products are detected (Fig. 4b, column 2 and 3), revealing that the process of  $\text{CO}_2$  reduction is initialized by photocatalysis. As presented in Fig. 4b, column 4, when Ar was used instead of  $\text{CO}_2$  to carry out the reaction under the identical condition, only a negligible amount of  $\text{H}_2$  is detected ( $1.41 \mu\text{mol}\cdot\text{h}^{-1}$ ), and almost no CO is produced. The above conclusion fully illustrates that the produced CO just stem from our introduced  $\text{CO}_2$ . In addition, a comparative test was performed with no TEOA added, and no gas products could be observed (Fig. 4b, column 5), indicating that the photoreduction  $\text{CO}_2$  process was significantly influenced by the sacrificial agent [59, 60]. As for the Co-Co LDH+TNS-15 sample, the yields of both CO ( $4.11 \mu\text{mol}\cdot\text{h}^{-1}$ ) and  $\text{H}_2$  ( $2.44 \mu\text{mol}\cdot\text{h}^{-1}$ ) were significantly lower than those of the Co-Co LDH/TNS-15 (Fig. 4b, column 6 and 7). Therefore, the results indicate the superiority of the distinctive nanoarray architecture.

Then, the wavelengths dependent photocatalytic activity was evaluated by five different incident light. The variation trend of the gas generation rate (Fig. 4c) is basically matched with the optical absorption spectra of  $[\text{Ru}(\text{bpy})_3]\text{Cl}_2\cdot 6\text{H}_2\text{O}$ , rather than that of the Co-Co LDH/TNS-15 catalysts (Fig. S9). These results further show that

our photoreduction CO<sub>2</sub> system is driven by the photoexcitation of [Ru(bpy)<sub>3</sub>]Cl<sub>2</sub>·6H<sub>2</sub>O, generating electrons to achieve the reduction process, wherein the Co-Co LDH/TNS-15 composite serves as a medium to accelerate electrons transmission to reduce CO<sub>2</sub> [16]. At the same time, the maximum AQE value is 0.92%, which is calculated at 420 nm. This value is higher than that of many other reported Co-based photocatalytic CO<sub>2</sub> reduction systems (Table S2). As presented in Fig. 4d, during the first 5h, the CO/H<sub>2</sub> yield is linear with the illumination time. However, the CO/H<sub>2</sub> generation rate gradually decreases after a long-term reaction, which could primarily be owing to the exhaustion of the photosensitizer [18, 59]. The cumulative yield of the gas product is approximately 65 μmol after 10 h irradiation. In order to confirm the decrease in activity caused by photosensitizer consumption, a five-hour set of cycle experiments were performed and fresh dyes were used each time. As displayed in Fig. 4e, the Co-Co LDH/TNS-15 catalyst holds good stability, the gas yield retains about 90% of its initial value after five cycles. Meanwhile, the XRD and XPS tests of the used catalysts were also performed to fully observe and confirm the stability. The measured sample still maintains the same XRD patterns and Co 2p spectra of the fresh sample (Fig. 4f, Fig. S10), revealing the superior reusability and stability of the Co-Co LDH/TNS-15 sample.

Photoelectrochemical characterizations were employed to clarify the deeply reasons for the better CO<sub>2</sub> photoreduction capability of Co-Co LDH/TNS-15 than pure Co-Co LDH in the viewpoint of charge transfer kinetics. On the one hand, the PL spectra was investigated to disclose the separation and recombination behavior of the photogenerated charges in the photocatalytic CO<sub>2</sub> reduction systems. As displayed in

Fig. 5a, the intensity is significantly decreased under the addition of catalysts in comparison with the blank system. Moreover, the emission intensity of the Co-Co LDH/TNS-15 is lower than that of the Co-Co LDH. The apparent PL quenching chiefly elucidates the outstandingly suppressed electron-hole recombination rate that improves the utilization of photoexcited electrons, thus boosting the catalytic efficiency [11, 61-63]. On the other hand, the EIS spectra was studied to further explore the electrons transport ability for different materials. As presented in Fig. 5b, the Co-Co LDH/TNS-15 exhibits a clearly smaller semicircle in the Nyquist plot, suggesting a lower electron-transfer resistance for the Co-Co LDH/TNS-15 hybrids that allows rapid transport and separation of interface charge, which is conducive for photoreduction  $\text{CO}_2$  [64-66]. These above data together confirm that the introduction of TNS obviously accelerates the electrons transfer and prolongs the lifetime of charge pairs, which is owing to the good conductivity of TNS and the fast separation rate of electron-hole pairs in hierarchical nanoarray architecture. Besides, the BET value of the Co-Co LDH/TNS-15 composite is slightly lower than the pristine Co-Co LDH (Fig. S11a, b), thereby the influence of the initial specific surface area of the material on the catalytic performance could be ruled out.

Accordingly, we put forward a rational mechanism for the photoreduction process. As shown in the Fig. 6, The photocatalytic reaction is initiated by the excitation of  $[\text{Ru}(\text{bpy})_3]\text{Cl}_2$  into the excited state ( $[\text{Ru}(\text{bpy})_3]\text{Cl}_2^*$ ) through irradiation, and then the  $[\text{Ru}(\text{bpy})_3]\text{Cl}_2^*$  is reductively quenched by the sacrificial electron donor (TEOA) to form a reduced state ( $[\text{Ru}(\text{bpy})_3]\text{Cl}_2^-$ ). Subsequently, the reduced  $[\text{Ru}(\text{bpy})_3]\text{Cl}_2^-$

transfers electrons to the Co-Co LDH/TNS composite, in which electrons could be rapidly transferred to the cobalt catalytically active sites through the complex interface. Finally, the adsorbed CO<sub>2</sub> on the active sites surface are activated and reduced to CO. At the same time, the protons in the solution are inevitably reduced to H<sub>2</sub> by excited electrons. Since the reaction starts from the [Ru(bpy)<sub>3</sub>]Cl<sub>2</sub>, the ability of electrons transport from [Ru(bpy)<sub>3</sub>]Cl<sub>2</sub> to Co-Co LDH/TNS is a necessary condition for the photoreduction of CO<sub>2</sub>. Hence, the Mott-Schottky test was performed to obtain the value of flat band potential for Co-Co LDH/TNS-15 composite. As displayed in Fig. S12a, the flat band potential is measured as *ca.* -1.01 V (*vs.* NHE), which is between the redox potential value of E (Ru(bpy)<sub>3</sub><sup>2+\*</sup>/Ru(bpy)<sub>3</sub><sup>+</sup>) = -1.09 V (*vs.* NHE) and E (CO<sub>2</sub>/CO) = -0.53 V (*vs.* NHE) [67, 68]. So, the Co-Co LDH/TNS-15 has an appropriate flat band potential that could receive the excited electrons from the reduced state [Ru(bpy)<sub>3</sub>]Cl<sub>2</sub><sup>-</sup>, thus reducing CO<sub>2</sub> to CO. Moreover, we investigated the energy level diagram (Fig. S12b) to completely understand the electrons transfer. The conduction band minimum (CBM) of Co-Co LDH/TNS-15 was calculated to be 3.33 eV relative to the vacuum level (see details in Fig. S12b). At the same time, the energy levels of [Ru(bpy)<sub>3</sub>]Cl<sub>2</sub> with respect to the vacuum level have been confirmed as 3.19 eV for the lowest unoccupied molecular orbital (LUMO) and 5.68 eV for the highest occupied molecular orbital (HOMO) in previous researches [10]. According to the above results, the CBM value of the Co-Co LDH/TNS-15 is lower than the LUMO value of [Ru(bpy)<sub>3</sub>]Cl<sub>2</sub>. Therefore, the photoexcited electrons can be easily transferred from the LUMO of photosensitizers to the conduction band of Co-Co LDH/TNS-15,

permitting the photocatalytic CO<sub>2</sub> reduction subsequently. In general, the Co-Co LDH/TNS hybrids possess two principal roles during the photocatalytic CO<sub>2</sub> reduction process: 1) hosting the active sites for the CO<sub>2</sub> photoreduction; 2) accelerating the transfer of electrons from the photosensitizer to the surface-active sites for the CO<sub>2</sub> reduction.

#### 4. Conclusions

In summary, ultrathin Co-Co LDH nanosheets strongly coupled with exfoliated Ti<sub>3</sub>C<sub>2</sub>T<sub>x</sub> MXenes were successfully achieved via the *in-situ* MOF-derived strategy. The optimized sample of hierarchical Co-Co LDH/TNS nanoarray is found to own obviously enhanced activity toward visible light driven CO<sub>2</sub> reduction, with a 2.2 times yield of CO (6.248 μmol h<sup>-1</sup>; 1.25×10<sup>4</sup> μmol h<sup>-1</sup> g<sup>-1</sup>) as compared with pristine Co-Co LDH nanosheets. This improvement may stem from the synergistic influences of highly conductive MXene species and the distinctive nanoarray architecture, which could lead to the rapid electron transfer and provide adequate catalytically active sites for the utilization of separated electrons. Simultaneously, the above Co-Co LDH/TNS hybrids exhibit a high AQE value (0.92%) and superb stability in the photocatalytic system. This study demonstrates a novel hierarchical nanoarray composite for efficient photocatalytic CO<sub>2</sub> reduction and also discloses that MXene serve as a vital role during photoreduction CO<sub>2</sub> process, which could be extended to other functional application. Furthermore, based on the consideration of real CO<sub>2</sub> concentration in the atmospheric environment, directly photoconversion of diluted CO<sub>2</sub> is the focus of future research.

#### Acknowledgements

This work was supported by the National Natural Science Foundation of China (Grant No. 21777046), the Guangdong Innovative and Entrepreneurial Research Team Program (No. 2016ZT06N569), Guangzhou Science and Technology Project (No. 201803030002).

## References:

- [1] R.D. Richardson, E.J. Holland, B.K. Carpenter, A renewable amine for photochemical reduction of CO<sub>2</sub>, *Nat. Chem.* 3 (2011) 301-303.
- [2] N.S. Lewis, D.G. Nocera, Powering the planet: Chemical challenges in solar energy utilization, *P. Natl. Acad. Sci. Usa.* 104 (2007) 20142.
- [3] D.M. Schultz, T.P. Yoon, Solar Synthesis: Prospects in Visible Light Photocatalysis, *Science* 343 (2014) 985.
- [4] R. Kuriki, M. Yamamoto, K. Higuchi, Y. Yamamoto, M. Akatsuka, D. Lu, S. Yagi, T. Yoshida, O. Ishitani, K. Maeda, Robust Binding between Carbon Nitride Nanosheets and a Binuclear Ruthenium(II) Complex Enabling Durable, Selective CO<sub>2</sub> Reduction under Visible Light in Aqueous Solution, *Angew. Chem. Int. Edit.* 56 (2017) 4867-4871.
- [5] W. Chen, X. Niu, S. An, H. Sheng, Z. Tang, Z. Yang, X. Gu, Emission and distribution of phosphine in paddy fields and its relationship with greenhouse gases, *Sci. Total Environ.* 599 (2017) 952-959.
- [6] K. R. Reddy, C. V. Reddy, M. N. Nadagouda, N. P. Shetti, S. Jaesool, T. M Aminabhavi, Polymeric graphitic carbon nitride (g-C<sub>3</sub>N<sub>4</sub>)-based semiconducting nanostructured materials: Synthesis methods, properties and photocatalytic applications, *J. Environ. Manage.* 238 (2019) 25-40.

- [7] Y. Wang, S. Wang, X. W. D. Lou, Dispersed Nickel Cobalt Oxyphosphide Nanoparticles Confined in Multichannel Hollow Carbon Fibers for Photocatalytic CO<sub>2</sub> Reduction, *Angew. Chem. Int. Edit.* 58 (2019) 1-6.
- [8] S. Cao, B. Shen, T. Tong, J. Fu, J. Yu, 2D/2D Heterojunction of Ultrathin MXene/Bi<sub>2</sub>WO<sub>6</sub> Nanosheets for Improved Photocatalytic CO<sub>2</sub> Reduction, *Adv. Funct. Mater.* 28 (2018) 1800136.
- [9] H. Takeda, O. Ishitani, Development of efficient photocatalytic systems for CO<sub>2</sub> reduction using mononuclear and multinuclear metal complexes based on mechanistic studies, *Coordin. Chem. Rev.* 254 (2010) 346-354.
- [10] W. Chen, B. Han, C. Tian, X. Liu, S. Liang, H. Deng, Z. Lin, MOFs-derived ultrathin holey Co<sub>3</sub>O<sub>4</sub> nanosheets for enhanced visible light CO<sub>2</sub> reduction, *Appl. Catal. B: Environ.* 244 (2019) 996-1003.
- [11] S. Wang, B.Y. Guan, X.W.D. Lou, Rationally designed hierarchical N-doped carbon @ NiCo<sub>2</sub>O<sub>4</sub> double-shelled nanoboxes for enhanced visible light CO<sub>2</sub> reduction, *Energ. Environ. Sci.* 11 (2018) 306-310.
- [12] B. Han, X. Ou, Z. Deng, Y. Song, C. Tian, H. Deng, Y. Xu, Z. Lin, Nickel Metal-Organic Framework Monolayers for Photoreduction of Diluted CO<sub>2</sub>: Metal-Node-Dependent Activity and Selectivity, *Angew. Chem. Int. Edit.* 57 (2018) 16811-16815.
- [13] C. Gao, Q. Meng, K. Zhao, H. Yin, D. Wang, J. Guo, S. Zhao, L. Chang, M. He, Q. Li, H. Zhao, X. Huang, Y. Gao, Z. Tang, Co<sub>3</sub>O<sub>4</sub> Hexagonal Platelets with Controllable Facets Enabling Highly Efficient Visible-Light Photocatalytic Reduction of CO<sub>2</sub>, *Adv. Mater.* 28 (2016) 6485-6490.
- [14] S. Wang, Z. Ding, X. Wang, A stable ZnCo<sub>2</sub>O<sub>4</sub> cocatalyst for photocatalytic CO<sub>2</sub> reduction, *Chem. Commun.* 51 (2015) 1517-1519.

- [15] Z. Wang, M. Jiang, J. Qin, H. Zhou, Z. Ding, Reinforced photocatalytic reduction of CO<sub>2</sub> to CO by a ternary metal oxide NiCo<sub>2</sub>O<sub>4</sub>, *Phys. Chem. Chem. Phys.* 17 (2015) 16040-16046.
- [16] S. Wang, W. Yao, J. Lin, Z. Ding, X. Wang, Cobalt imidazolate Metal-Organic frameworks photosplit CO<sub>2</sub> under mild reaction conditions, *Angew. Chem. Int. Edit.* 53 (2014) 1034-1038.
- [17] K. Zhao, S. Zhao, C. Gao, J. Qi, H. Yin, D. Wei, M. F. Mideksa, X. Wang, Y. Gao, Z. Tang, R. Yu, Metallic Cobalt-Carbon composite as recyclable and robust magnetic photocatalyst for efficient CO<sub>2</sub> reduction, *Small* 14 (2018) 1800762.
- [18] X. Lin, Y. Gao, M. Jiang, Y. Zhang, Y. Hou, W. Dai, S. Wang, Z. Ding, Photocatalytic CO<sub>2</sub> reduction promoted by uniform perovskite hydroxide CoSn(OH)<sub>6</sub> nanocubes, *Appl. Catal. B: Environ.* 224 (2018) 1009-1016.
- [19] J. Qin, S. Wang, X. Wang, Visible-light reduction CO<sub>2</sub> with dodecahedral zeolitic imidazolate framework ZIF-67 as an efficient co-catalyst, *Appl. Catal. B: Environ.* 209 (2017) 476-482.
- [20] J. M. Lehn, R. Ziessel, Photochemical generation of carbon monoxide and hydrogen by reduction of carbon dioxide and water under visible light irradiation, *P. Natl. Acad. Sci. Usa.* 79 (1982) 701-704.
- [21] S. Wang, Y. Hou, X. Wang, Development of a Stable MnCo<sub>2</sub>O<sub>4</sub> Cocatalyst for Photocatalytic CO<sub>2</sub> Reduction with Visible Light, *ACS Appl. Mater. Inter.* 7 (2015) 4327-4335.
- [22] T. Sakakura, J. Choi, H. Yasuda, Transformation of carbon dioxide, *Chem. Rev.* 107 (2007) 2365-2387.
- [23] Q. Mu, W. Zhu, G. Yan, Y. Lian, Y. Yao, Q. Li, Y. Tian, P. Zhang, Z. Deng, Y. Peng, Activity and selectivity regulation through varying the size of cobalt active sites in photocatalytic CO<sub>2</sub> reduction, *J. Mater. Chem. A.* 6 (2018) 21110-21119.

- [24] N. L. Reddy, V. N. Rao, M. M. Kumari, R. R. Kakarla, P. Ravi, M. Sathish, M. Karthik, S. M. Venkatakrishnan, Inamuddin, Nanostructured semiconducting materials for efficient hydrogen generation, *Environ. Chem. Lett.* 16 (2018) 765-796.
- [25] N. L. Reddy, V. N. Rao, M. Vijayakumar, R. Santhosh, S. Anandan, M. Karthik, M. V. Shankar, K. R. Reddy, N. P. Shetti, M. N. Nadagouda, T. M. Aminabhavi, A review on frontiers in plasmonic nano-photocatalysts for hydrogen production, *Int. J. Hydrogen Energ.* 44 (2019) 10453-10472.
- [26] M. Tahir, B. Tahir, M. G. M. Nawawi, M. Hussain, A. Muhammad, Cu-NPs embedded 1D/2D CNTs/pCN heterojunction composite towards enhanced and continuous photocatalytic CO<sub>2</sub> reduction to fuels, *Appl. Surf. Sci.* 485 (2019) 450-461.
- [27] W. Yu, D. Xu, T. Peng, Enhanced photocatalytic activity of g-C<sub>3</sub>N<sub>4</sub> for selective CO<sub>2</sub> reduction to CH<sub>3</sub>OH via facile coupling of ZnO: a direct Z-scheme mechanism, *J. Mater. Chem. A* 3 (2015) 19936-19947.
- [28] Q. Xiang, J. Yu, M. Jaroniec, Graphene-based semiconductor photocatalysts, *Chem. Soc. Rev.* 41 (2012) 782-796.
- [29] M. Naguib, M. Kurtoglu, V. Presser, J. Lu, J. Niu, M. Heon, L. Hultman, Y. Gogotsi, M. W. Barsoum, Two-Dimensional nanocrystals produced by exfoliation of Ti<sub>3</sub>AlC<sub>2</sub>, *Adv. Mater.* 23 (2011) 4248-4253.
- [30] X. Wu, Z. Wang, M. Yu, L. Xiu, J. Qiu, Stabilizing the MXenes by carbon nanoplating for developing hierarchical nanohybrids with efficient lithium storage and hydrogen evolution capability, *Adv. Mater.* 29 (2017) 1607017.
- [31] M. R. Lukatskaya, O. Mashtalir, C. E. Ren, Y. Dall'Agnese, P. Rozier, P. L. Taberna, M. Naguib, P. Simon, M. W. Barsoum, Y. Gogotsi, Cation intercalation and high volumetric

capacitance of Two-Dimensional titanium carbide, *Science* 341 (2013) 1502-1505.

[32] Z. Ling, C. E. Ren, M. Zhao, J. Yang, J. M. Giammarco, J. Qiu, M. W. Barsoum, Y. Gogotsi, Flexible and conductive MXene films and nanocomposites with high capacitance, *P. Natl. Acad. Sci. Usa.* 111 (2014) 16676-16681.

[33] M. Zhao, X. Xie, C. E. Ren, T. Makaryan, B. Anasori, G. Wang, Y. Gogotsi, Hollow MXene spheres and 3D macroporous MXene frameworks for Na-Ion storage, *Adv. Mater.* 29 (2017) 1702410.

[34] S. Kang, M. Shang, M. A. Spence, M. Andrew, S. Liu, J. Niu, Dynamic charge acceptance and hydrogen evolution of a new MXene additive in advanced lead-acid batteries via a rapid screening three-electrode method, *Chem. Commun.* 54 (2018) 3456-3459.

[35] B. Anasori, M. R. Lukatskaya, Y. Gogotsi, 2D metal carbides and nitrides (MXenes) for energy storage, *Nat. Rev. Mater.* 2 (2017) 16098.

[36] H. Lin, X. Wang, L. Yu, Y. Chen, J. Shi, Two-Dimensional ultrathin MXene ceramic nanosheets for photothermal conversion, *Nano Lett.* 17 (2017) 384-391.

[37] M. Ghidui, M. R. Lukatskaya, M. Zhao, Y. Gogotsi, M. W. Barsoum, Conductive two-dimensional titanium carbide 'clay' with high volumetric capacitance, *Nature* 516 (2014) 78-171.

[38] Y. Peng, B. Akuzum, N. Kurra, M. Zhao, M. Alhabe, B. Anasori, E. C. Kumbur, H. N. Alshareef, M. Ger, Y. Gogotsi, All-MXene (2D titanium carbide) solid-state microsupercapacitors for on-chip energy storage, *Energ. Environ. Sci.* 9 (2016) 2847-2854.

[39] J. Ran, G. Gao, F. Li, T. Ma, A. Du, S. Qiao,  $Ti_3C_2$  MXene co-catalyst on metal sulfide photo-absorbers for enhanced visible-light photocatalytic hydrogen production, *Nat. Commun.* 8 (2017) 13907.

- [40] X. Xie, N. Zhang, Z. Tang, M. Anpo, Y. Xu,  $\text{Ti}_3\text{C}_2\text{Tx}$  MXene as a Janus cocatalyst for concurrent promoted photoactivity and inhibited photocorrosion, *Appl. Catal. B: Environ.* 237 (2018) 43-49.
- [41] K. R. Reddy, M. Hassan, V. G. Gomes, Hybrid nanostructures based on titanium dioxide for enhanced photocatalysis, *Appl. Catal. A-Gen.* 489 (2015) 1-16.
- [42] S. Wang, B. Y. Guan, X. Wang, X. W. D. Lou, Formation of Hierarchical  $\text{Co}_9\text{S}_8@\text{ZnIn}_2\text{S}_4$  Heterostructured Cages as an Efficient Photocatalyst for Hydrogen Evolution, *J. Am. Chem. Soc.* 140 (2018) 15145-15148.
- [43] H. Zhang, Ultrathin Two-Dimensional nanomaterials, *ACS Nano.* 9 (2015) 9451-9469.
- [44] H. Gao, J. Wang, M. Jia, F. Yang, R. S. Andriamitantoa, X. Huang, W. Dong, G. Wang, Construction of  $\text{TiO}_2$  nanosheets/tetra (4-carboxyphenyl) porphyrin hybrids for efficient visible-light photoreduction of  $\text{CO}_2$ , *Chem. Eng. J.* 374 (2019) 684-693.
- [45] Y. Bai, P. Yang, L. Wang, B. Yang, H. Xie, Y. Zhou, L. Ye, Ultrathin  $\text{Bi}_4\text{O}_5\text{Br}_2$  nanosheets for selective photocatalytic  $\text{CO}_2$  conversion into CO. *Chem. Eng. J.* 360 (2019) 473-482.
- [46] Z. Sun, N. Talreja, H. Tao, J. Texter, M. Muhler, J. Strunk, J. Chen, Catalysis of carbon dioxide photoreduction on nanosheets: Fundamentals and challenges, *Angew. Chem. Int. Edit.* 57 (2018) 7610-7627.
- [47] Y. Zhou, Y. Zhang, M. Lin, J. Long, Z. Zhang, H. Lin, J. C. Wu, X. Wang, Monolayered  $\text{Bi}_2\text{WO}_6$  nanosheets mimicking heterojunction interface with open surfaces for photocatalysis, *Nat. Commun.* 6 (2015) 8430.
- [48] J. Zhang, Y. Chen, X. Wang, Two-dimensional covalent carbon nitride nanosheets: Synthesis, functionalization, and applications, *Energ. Environ. Sci.* 8 (2015) 3092-3108.

- [49] S. Qamar, F. Lei, L. Liang, S. Gao, K. Liu, Y. Sun, W. Ni, Y. Xie, Ultrathin TiO<sub>2</sub> flakes optimizing solar light driven CO<sub>2</sub> reduction, *Nano Energy* 26 (2016) 692-698.
- [50] P. Xia, B. Zhu, J. Yu, S. Cao, M. Jaroniec, Ultra-thin nanosheet assemblies of graphitic carbon nitride for enhanced photocatalytic CO<sub>2</sub> reduction, *J. Mater. Chem. A* 5 (2017) 3230-3238.
- [51] X. Wu, Z. Lu, W. Zhu, Q. Yang, G. Zhang, J. Liu, X. Sun, High-performance aqueous battery with double hierarchical nanoarrays, *Nano Energy* 10 (2014) 229-234.
- [52] N. Abushrenta, X. Wu, J. Wang, J. Liu, X. Sun, Hierarchical co-based porous layered double hydroxide arrays derived via alkali etching for high-performance supercapacitors, *Sci. Rep.* 5 (2015) 13082.
- [53] H. Zou, B. He, P. Kuang, J. Yu, K. Fan, Metal-Organic Framework-Derived Nickel-Cobalt sulfide on ultrathin mxene nanosheets for electrocatalytic oxygen evolution, *ACS Appl. Mater. Inter.* 10 (2018) 22311-22319.
- [54] X. Bai, J. Liu, Q. Liu, R. Chen, X. Jing, B. Li, J. Wang, In-Situ fabrication of MOF-Derived Co-Co layered double hydroxide hollow Nanocages/Graphene composite: A novel electrode material with superior electrochemical performance, *Chem. Eur. J.* 23 (2017) 14839-14847.
- [55] J. Low, L. Zhang, T. Tong, B. Shen, J. Yu, TiO<sub>2</sub>/MXene Ti<sub>3</sub>C<sub>2</sub> composite with excellent photocatalytic CO<sub>2</sub> reduction activity, *J. Catal.* 361 (2018) 255-266.
- [56] X. Zhao, M. Liu, Y. Chen, B. Hou, N. Zhang, B. Chen, N. Yang, K. Chen, J. Li, L. An, Fabrication of layered Ti<sub>3</sub>C<sub>2</sub> with an accordion-like structure as a potential cathode material for high performance lithium-sulfur batteries, *J. Mater. Chem. A* 3 (2015) 7870-7876.
- [57] R. Meng, J. Huang, Y. Feng, L. Zu, C. Peng, L. Zheng, L. Zheng, Z. Chen, G. Liu, B. Chen, Y. Mi, J. Yang, Black phosphorus quantum Dot/Ti<sub>3</sub>C<sub>2</sub> MXene nanosheet composites for efficient

- electrochemical Lithium/Sodium-Ion storage, *Adv. Energy Mater.* 8 (2018) 1801514.
- [58] Z. Zeng, Y. Yan, J. Chen, P. Zan, Q. Tian, P. Chen, Boosting the photocatalytic ability of Cu<sub>2</sub>O nanowires for CO<sub>2</sub> conversion by MXene quantum dots, *Adv. Funct. Mater.* 29 (2019) 1806500.
- [59] Y. Wang, N. Huang, J. Shen, P. Liao, X. Chen, J. Zhang, Hydroxide ligands cooperate with catalytic centers in Metal-Organic frameworks for efficient photocatalytic CO<sub>2</sub> reduction, *J. Am. Chem. Soc.* 140 (2018) 38-41.
- [60] H. Xu, J. Hu, D. Wang, Z. Li, Q. Zhang, Y. Luo, S. Yu, H. Jiang, Visible-Light photoreduction of CO<sub>2</sub> in a Metal-Organic framework: Boosting Electron-Hole separation via electron trap states, *J. Am. Chem. Soc.* 137 (2015) 13440-13443.
- [61] C. V. Reddy, I. N. Reddy, K. R. Reddy, S. Jaesool, K. Yoo, Template-free synthesis of tetragonal Co-doped ZrO<sub>2</sub> nanoparticles for applications in electrochemical energy storage and water treatment *Electrochim. Acta.* 317 (2019) 416-426.
- [62] B. Han, J. Song, S. Liang, W. Chen, H. Deng, X. Ou, Y. Xu, Z. Lin, Hierarchical NiCo<sub>2</sub>O<sub>4</sub> hollow nanocages for photoreduction of diluted CO<sub>2</sub>: Adsorption and active sites engineering, *Appl. Catal. B: Environ.* 260 (2020) 118208.
- [63] C. Venkata Reddy, I. N. Reddy, B. Akkinapally, K. R. Reddy, J. Shim, Synthesis and photoelectrochemical water oxidation of (Y, Cu) codoped  $\alpha$ -Fe<sub>2</sub>O<sub>3</sub> nanostructure photoanode, *J. Alloy. Compd.* 814 (2020) 152349.
- [64] S. Wang, B. Y. Guan, X. W. D. Lou, Construction of ZnIn<sub>2</sub>S<sub>4</sub>-In<sub>2</sub>O<sub>3</sub> hierarchical tubular heterostructures for efficient CO<sub>2</sub> photoreduction, *J. Am. Chem. Soc.* 140 (2018) 5037-5040.
- [65] S. Wang, B. Y. Guan, Y. Lu, X. W. D. Lou, Formation of hierarchical In<sub>2</sub>S<sub>3</sub>-CdIn<sub>2</sub>S<sub>4</sub> heterostructured nanotubes for efficient and stable visible light CO<sub>2</sub> reduction, *J. Am. Chem. Soc.*

139 (2017) 17305-17308.

[66] C. Yang, Q. Li, Y. Xia, K. Lv, M. Li, Enhanced visible-light photocatalytic CO<sub>2</sub> reduction performance of ZnIn<sub>2</sub>S<sub>4</sub> microspheres by using CeO<sub>2</sub> as cocatalyst, Appl. Surf. Sci. 464 (2019) 388-395.

[67] N. S. C Creutz, Reductive quenching of the tris (2, 2'-bipyridine) ruthenium (II) luminescence, Inorg. Chem. 15 (1976) 2.

[68] J. Schneider, H. Jia, J. T. Muckerman, E. Fujita, Thermodynamics and kinetics of CO<sub>2</sub>, CO, and H<sup>+</sup> binding to the metal center of CO<sub>2</sub> reduction catalysts, Chem. Soc. Rev. 41 (2012) 2036-2051.

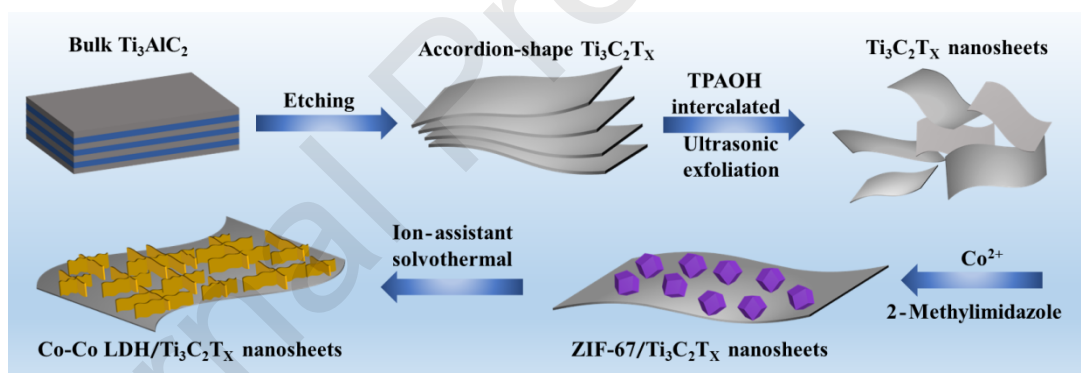


Fig. 1. Schematic illustration of the synthetic process of Co-Co LDH/TNS nanosheets.

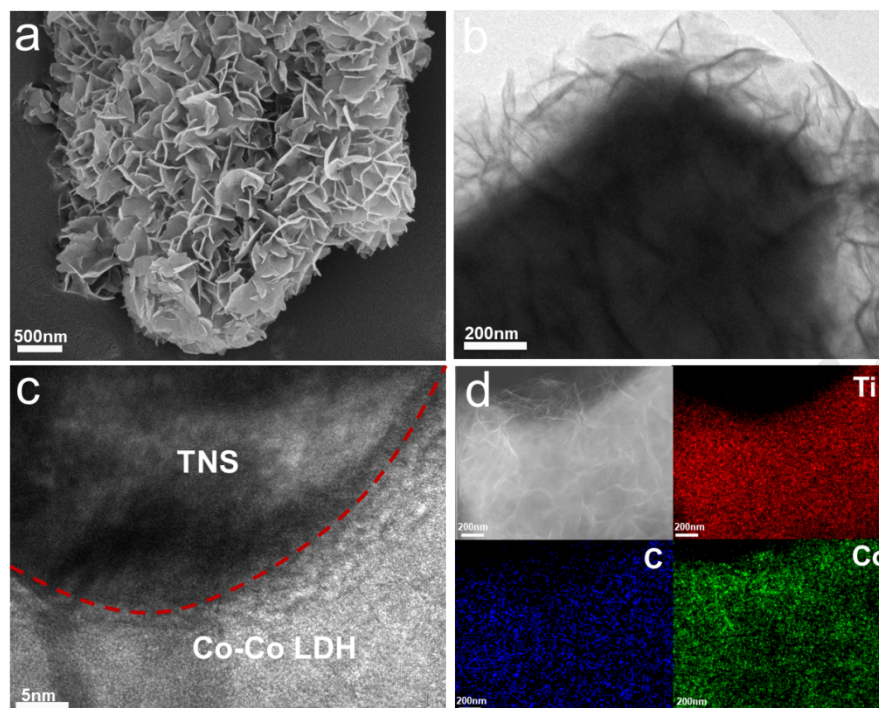


Fig. 2. (a) SEM image, (b) TEM image, (c) HRTEM image, and (d) EDX mapping images of Co-Co LDH/TNS-15.

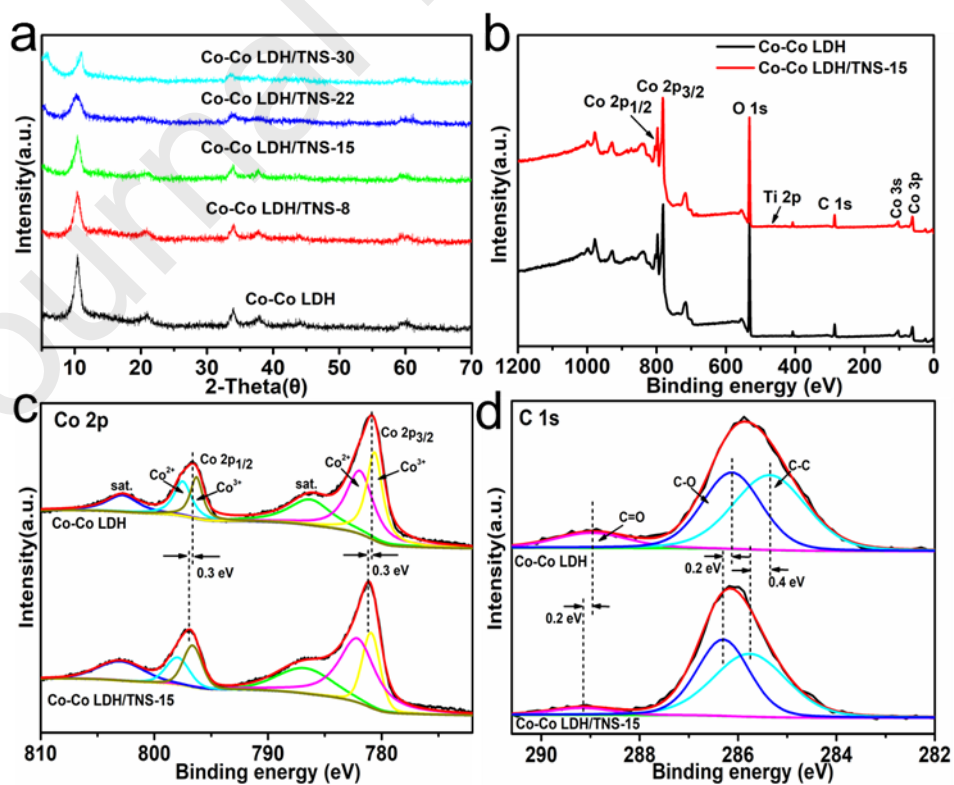


Fig. 3. (a) XRD patterns of Co-Co LDH/TNS hybrids with different TNS content in the samples. (b) XPS survey spectra, (c) high-resolution XPS Co 2p spectra, and (d) high-resolution XPS C 1s spectra of Co-Co LDH and Co-Co LDH/TNS-15.

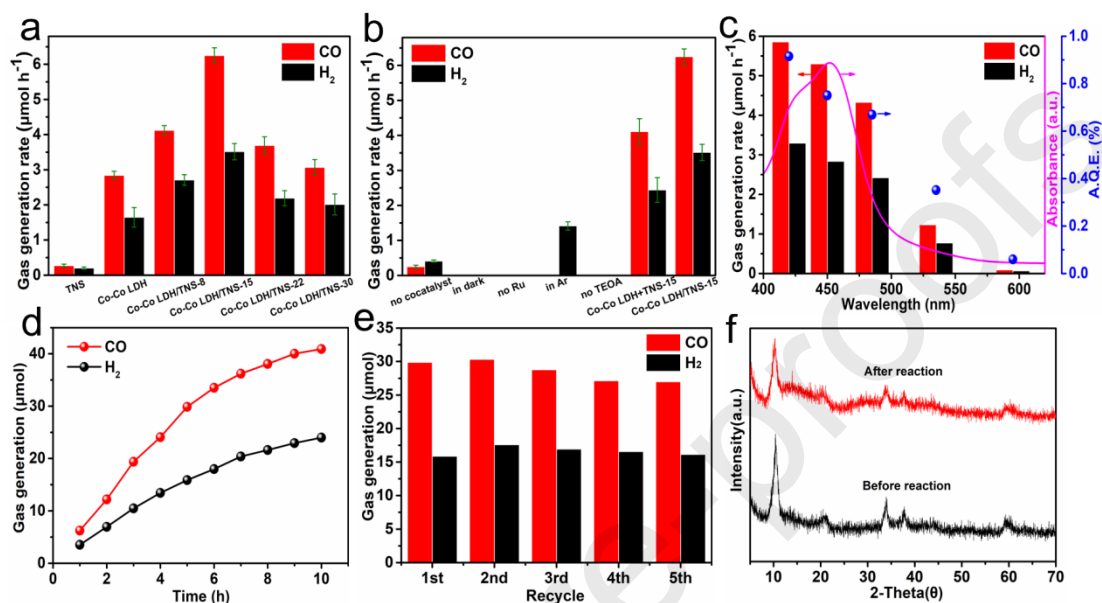


Fig. 4. (a) Photocatalytic activity of Co-Co LDH/TNS hybrids with different TNS content in the samples. (b) Generation of CO and  $\text{H}_2$  under various reaction conditions. (c) Wavelength-dependent of the CO and  $\text{H}_2$  production. The line is the absorption spectrum of the Ru photosensitizer. The dots are the A.Q.E. value for each wavelength. (d) Evolution of CO and  $\text{H}_2$  as a function of reaction time. (e) Generation of CO and  $\text{H}_2$  in stability tests (the time of each cycle is 5 h). (f) XRD patterns of Co-Co LDH/TNS-15 hybrids before and after  $\text{CO}_2$  photoreduction reaction.

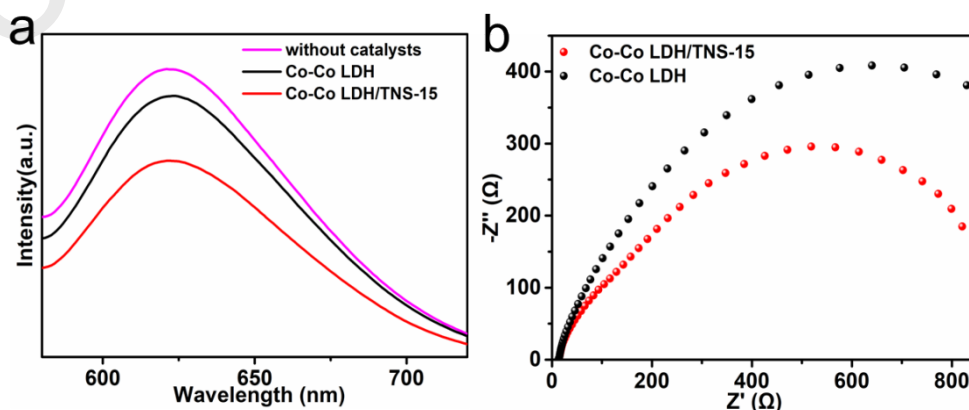


Fig. 5. (a) PL spectra of the photocatalytic CO<sub>2</sub> reduction systems with Co-Co LDH, Co-Co LDH/TNS-15 and without catalysts at room temperature. (b) Nyquist diagram of electrochemical impedance spectra for Co-Co LDH and Co-Co LDH/TNS-15 modified ITO electrode.

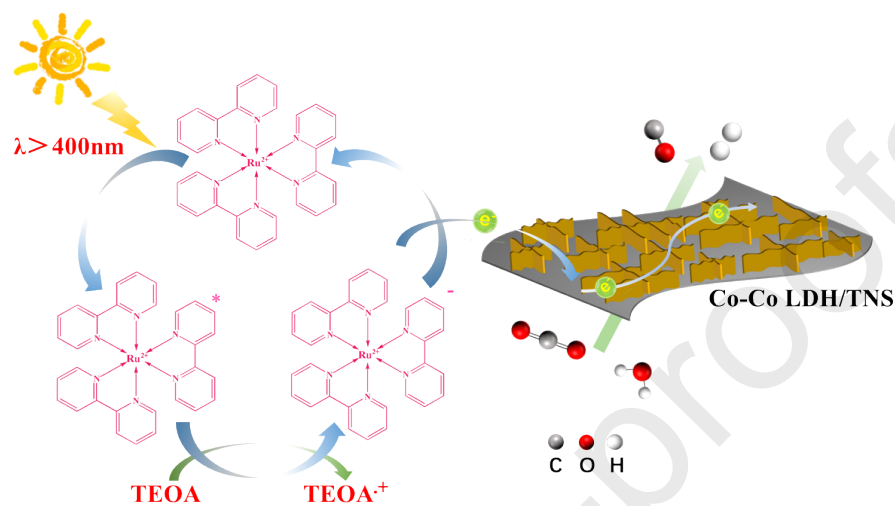
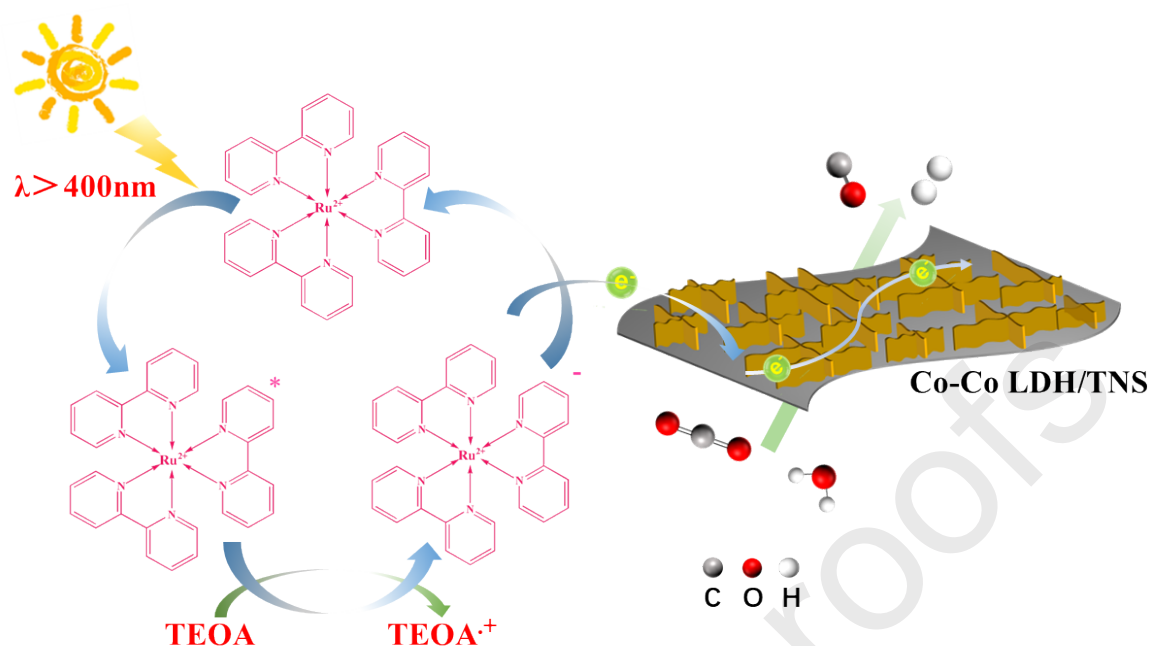


Fig. 6. Proposed photocatalytic mechanism of Co-Co LDH/TNS composite with [Ru(bpy)<sub>3</sub>]Cl<sub>2</sub> for the visible-light-driven photocatalytic CO<sub>2</sub> reduction reaction.



Highlight:

The Co-Co LDH/TNS nanoarray was synthesized via an in situ MOF-derived strategy.

The composite remarkably facilitate the migration and separation of charge carriers.

The composite displays an excellent photocatalytic performance for CO<sub>2</sub> conversion.

Conflict of interest

We declare that we do not have any commercial or associative interest that represents a conflict of interest in connection with the work submitted.